J Mater Sci (2008) 43:4583–4591
DOI 10.1007/s10853-008-2681-3

Marangoni convection and weld shape variations in He–CO_2 shielded gas tungsten arc welding on SUS304 stainless steel

Shanping Lu · Hidetoshi Fujii · Kiyoshi Nogi

Received: 10 January 2008 / Accepted: 25 April 2008 / Published online: 13 May 2008

Abstract Bead-on-plate GTA welding (gas tungsten arc welding) on a SUS304 substrate is carried out to investigate the effect of carbon dioxide gas in the helium base shielding on the oxygen content in the weld pool and the weld shape variations. Experimental results show that small addition of carbon dioxide to the shielding gas can precisely adjust the weld metal oxygen content and change the weld shape from wide shallow type to narrow deep one when the weld pool oxygen content is over the critical value, which is from 68 to 82 ppm, due to the Marangoni convection reversal from the outward to inward mode on the pool surface. The weld depth/width ratio increases two times suddenly when the carbon dioxide content in the torch gas is over 0.4 or 0.2% for 1 mm or 3 mm arc length, respectively. The GTA weld shape depends to a large extent on the pattern and magnitude of the Marangoni convection on the pool surface, which is influenced by the active element oxygen content in the SUS304 pool, temperature coefficient of the surface tension ($d\sigma/dT$), and the temperature gradient on the pool surface (dT/dr, r is the radius of the weld pool surface). Changing the welding parameters will alter the temperature distribution and gradient on the pool surface, and thus, affect the magnitude of the Marangoni convection and the final weld shape.

S. Lu · H. Fujii · K. Nogi
Joining and Welding Research Institute, Osaka University, Osaka 567-0047, Japan

S. Lu (✉)
Shenyang National Laboratory for Materials Science, Institute of Metal Research, Chinese Academy of Science, Shenyang 110016, People's Republic of China
e-mail: shplu@imr.ac.cn

Introduction

Gas tungsten arc welding (GTAW), also called tungsten inert gas welding (TIG), is one of the main welding methods which has been widely used in industry for the welding of stainless steel, titanium alloy, and other non-ferrous metals for its high weld quality, lower sensitivity to the joint fitting and welding parameters, and lower equipment investment. However, compared to high energy welding method, such as laser welding, electronic beam welding, and plasma welding, the single pass GTAW penetration is shallow and X or V type grooves are necessary in welding thick plates, which makes the welding productivity low.

Increasing the GTAW penetration has been a concern for decades, and several technologies were proposed including the adjustment to the minor elements in the raw material, such as the sulfur, oxygen, selenium, and bismuth in group VIB and fluorine, bromine, and chlorine in group VIIB [1–8], smearing active fluxes on the plate surface (A-TIG or FB-TIG) before welding [7, 9–28], and adding a small amount of active gas to the inert shielding gas [29–35] to obtain deep penetration. Even though some techniques have been partially applied in industry, there is still no common agreement on the mechanism of A-TIG welding. There have been four proposed mechanisms to explain A-TIG phenomena. The first is based on the concept that the surface tension of a molten pool lowers and the pool surface is likely to descend due to the arc pressure, resulting in arc concentration at the descended portion of the pool. This mechanism is called the TIG keyhole model [36]. In the second mechanism, it is considered that vaporized flux molecules contract the welding arc [19–23, 26, 27, 37, 38]. The third one is based on the following hypothesis: the reverse Marangoni convection is induced

by the change of the temperature coefficient of the surface tension (dσ/dT) from negative to positive when the concentration of a surface active element in the weld pool exceeds a critical value [6, 7, 18, 40–43]. Recently, Lowke et al. [44] proposed the fourth mechanism called the insulation mode.

Former research works showed that by smearing oxide fluxes [24, 25] or adding small amount active gas, O_2 or CO_2 [32–34], to the argon shielding gas can significantly increase the GTAW penetration into SUS304 stainless steel. It is found that the active element, oxygen, in the weld pool can be adjusted by smearing the oxide flux or adding small amount of active gas to the Ar shielding. When the oxygen content is over a critical value, the reverse Marangoni convection is induced and a deep narrow weld shape is obtained. However, the weld shape is sensitive to the quantity of the smearing oxide flux before welding, and it is difficult for the operator to control the quantity of flux used. However, the amount of oxygen content in a weld pool can be easily controlled by adding active gas to the argon shielded gas than by smearing oxide flux on plates.

Helium is another inert gas for GTA welding. The thermal conductivity is higher for He gas (460 mW/mK) than that for Ar gas (53 mW/mK). To maintain arc thermal equilibrium, the He arc is more constricted than the Ar arc. The current density in the He arc and at the anode spot is also high. Therefore, the use of He gas should increase the electromagnetic force and possibly raise the temperature gradient on the pool surface (dT/dr). Since the intensity of the Marangoni convection is governed by the combined effect of the temperature gradient on the pool surface (dT/dr) and the temperature coefficient of the surface tension (dσ/dT), He arc should affect the Marangoni convection more significantly than the Ar arc. In this article, experimental studies are carried out to investigate the effect of He–CO_2 mixed shielding gas on the weld pool oxygen content, Marangoni convection, and weld shape variations with different welding parameters. It is benefit to accumulate the experimental data for future real application in industry with a high GTA welding efficiency.

Experimental

Bead-on-plate welding was carried out on SUS304 stainless steel substrate (100 × 50 × 10 mm^3) with the average composition of 0.06%C, 0.44%Si, 0.96%Mn, 8.19%Ni, 18.22%Cr, 0.027%P, 0.0005%S, and 0.0038%O and the rest of Fe. Prior to the welding, the surface of the plate was ground using an 80-grit flexible abrasive paper and then cleaned with acetone.

A water-cooled torch with a thoriated tungsten electrode (W-2%ThO_2, 2.4 mm diameter) was used in the experiments by direct current, electrode negative (DCEN) polarity power source (YC-300BZ1) with a mechanized system in which the test piece moves at a set speed. The shielding gas was He–CO_2 mixed gas with the CO_2 content from 0 to 1.0%. The effects of welding parameters on the weld shape are also investigated using pure He and He–0.6%CO_2 shielding gases with welding current from 80 to 250 A and welding speed from 0.75 to 5.0 mm/s. Table 1 shows the welding conditions used in the trial.

Table 1 Welding parameters

Parameters	Value
Electrode type	DCEN, W-2%ThO_2
Diameter of electrode	2.4 mm
Vertex angle of electrode	60°
Shield gas	He, He–CO_2
Gas flow rate	10 L/min
Bead length	50 mm
Spot time	3 s
Arc length	1 mm, 3 mm
Welding current	80–250 A
Welding speed	0.75–5.0 mm/s

After welding, all the weld beads were sectioned and the specimens for the weld shape observation were prepared by etching using HCl (50 mL) + Cu_2SO_4 (25 mL) solution to reveal the bead shape and dimensions. The cross-sections of the weld bead were photographed using an optical microscope (Olympus HC300 Z/OL). The oxygen content in the weld metal was analyzed using an oxygen/nitrogen analyzer (Horiba, EMGA-520). Samples for the oxygen measurements were cut directly from the weld metal.

Results and discussion

Weld shape and Marangoni convection

The effect of the torch gas carbon dioxide content on the weld shape and oxygen solution in the weld pool is studied at 160 A welding current and 2 mm s^{-1} welding speed. The arc length was set at 1 and 3 mm. The torch gas concentration was varied between pure helium and helium with 1.0%CO_2. Figures 1 and 2 show representative weld cross-sections under different torch gas shielding conditions from pure He to He–1.0%CO_2 with 1 and 3 mm arc length, respectively. At 1 mm arc length, the weld shape suddenly changes from wide shallow type to narrow deep one as the carbon dioxide in the shielding is over 0.4% as shown in Fig. 1e–h. When the torch gas carbon dioxide content is over 0.2% for 3 mm arc length, the weld penetration becomes deep as shown in Fig. 2c–h.

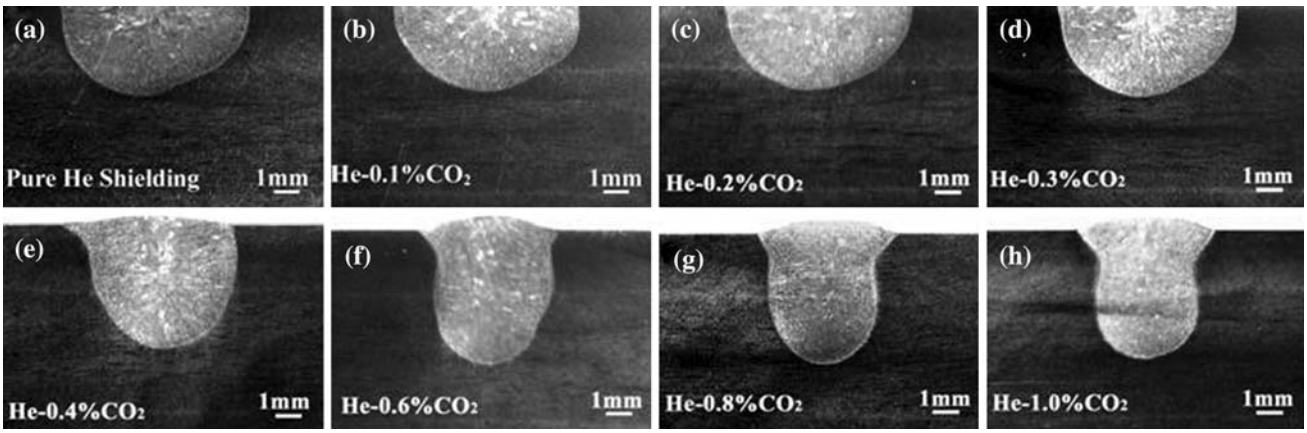

Fig. 1 Weld shapes under different He–CO_2 shielding with 1 mm arc length

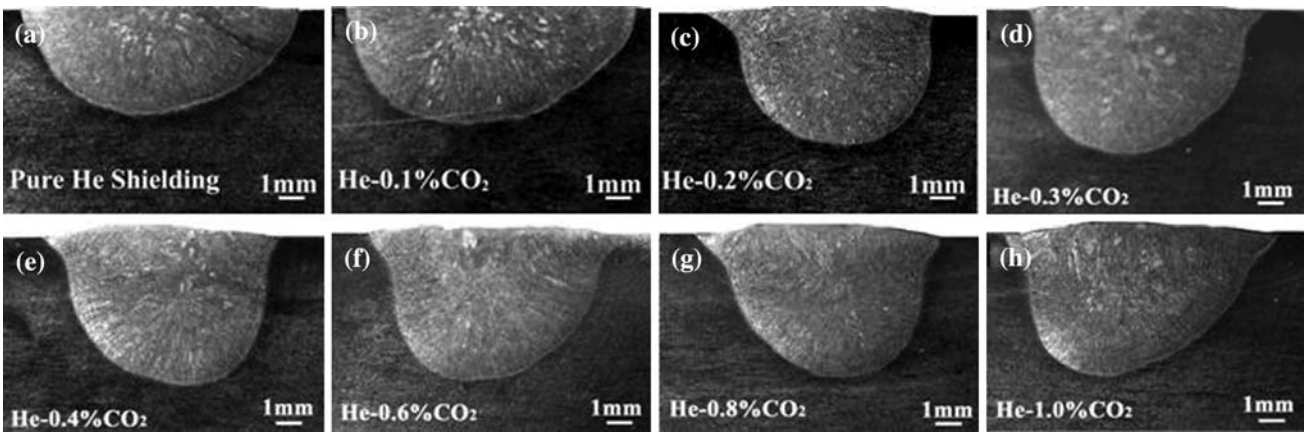

Fig. 2 Weld shapes under different He–CO_2 shielding with 3 mm arc length

Figures 3 and 4 show the effect of the torch gas carbon dioxide content on the weld depth/width (D/W) ratio and the weld metal oxygen content when 1 and 3 mm arc length are used, respectively. The weld D/W ratio is suddenly increased from 0.5 to 0.95 when the carbon dioxide content is over 0.4% in the He shielding gas for the 1 mm arc length as shown in Fig. 3. Figure 4 gives the experimental result when 3 mm arc length is used. The weld D/W ratio increases abruptly from 0.35 to 0.60 when the torch gas carbon dioxide content is more than 0.2%. It is found that the weld metal oxygen content monotonously increases with the increasing torch gas carbon dioxide content, and the weld metal oxygen content can be precisely adjusted by the small addition of CO_2 gas into He shielding gas.

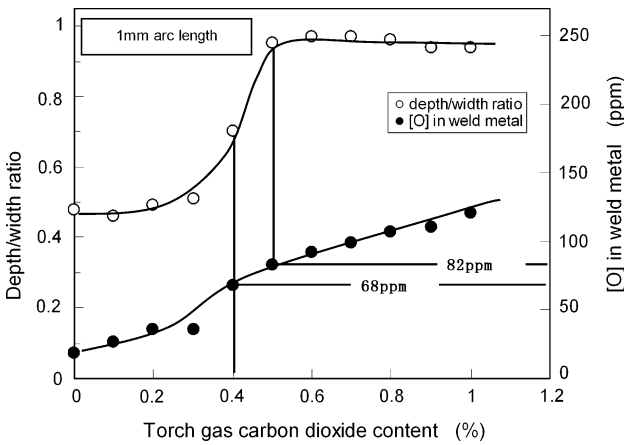

Fig. 3 Weld depth/width ratio and weld metal oxygen content under different He–CO_2 shielding with 1 mm arc length

Generally, the weld shape is controlled via heat transfer by a combination of convection and conduction in the liquid pool. The relative importance between the heat convection and conduction, which can be valued by Peclet number, varies for different materials and represents the ratio of heat transfer by convection and conduction. It is defined as follows: $Pe = L \cdot V_{max}/2\alpha_l$, where, V_{max} is the maximum surface velocity, α_l is the thermal diffusivity of liquid, and L is the characteristic length of the weld pool, which can be taken as the weld pool surface radius for wide and shallow weld pool without or with low active element content. In a

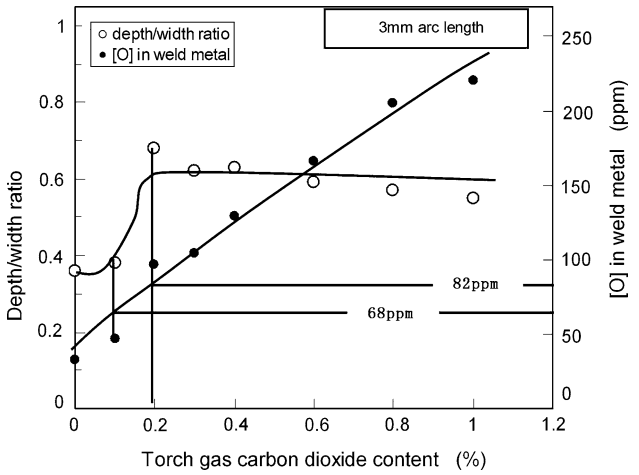

Fig. 4 Weld depth/width ratio and weld metal oxygen content under He–CO_2 shielding with 3 mm arc length

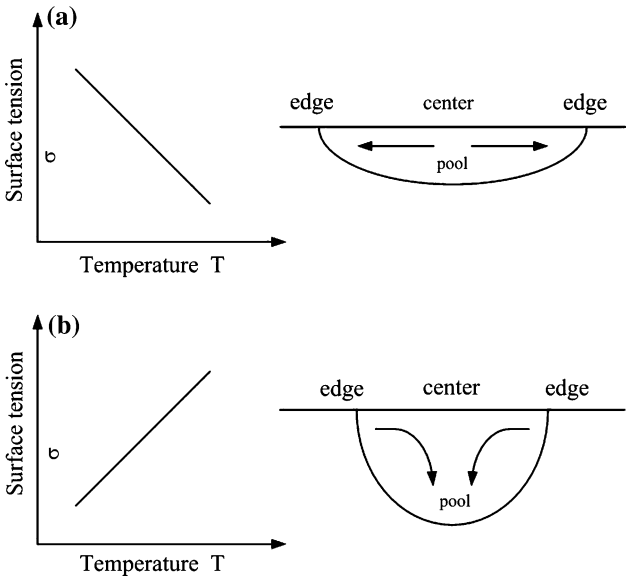

Fig. 5 Marangoni convection mode in the weld pool (**a**) $\partial\sigma/\partial T < 0$; (**b**) $\partial\sigma/\partial T > 0$

deep and narrow weld pool containing certain active element, L can be taken as the depth of the weld pool [33]. Here, two representative weld shapes, Fig. 1c and g, are selected to calculate the Peclet number. The weld pool surface radius for Fig. 1c is 3.61 mm, and weld depth for Fig. 1g is 5.09 mm. The other thermal properties for SUS304 are from published reference [33]. The calculated Peclect numbers are 55.5 and 78.3 for Fig. 1c and g, respectively. Research by Limmaneevichitr and Kou [45] showed that the heat transfer in the weld pool is dominated by conduction for $Pe \ll 1$, and on the other hand, for $Pe \gg 1$, the heat transfer in the weld pool is dominated by convection. The high Peclet number signifies that heat transfer in liquid pool in this study is dominated by the convection mode. Therefore, the GTA weld shapes here depend to a large extent on the fluid flow mode in the welding pool, which was governed by the combined effect of the electromagnetic force, surface tension, buoyancy force, and impinging force of the arc plasma. Many research works have shown that the Marangoni convection induced by the surface tension on the pool surface is the main convection that significantly influences the fluid flow in a liquid pool [6, 7, 18, 39–43, 46]. Generally, the surface tension decreases with the increasing temperature, that is $\partial\sigma/\partial T<0$, for a pure metal and many alloys. Since there is a large temperature gradient on the welding pool surface, a large surface tension gradient arises along the surface. In the weld pool of such materials, the surface tension is higher at the cooler pool edges than that on the pool center. Hence, the Marangoni convection flows from the pool center to the edges. The heat flux from the arc is readily transferred from the pool center to the edges and the weld shape becomes relatively wide and shallow as shown in Fig. 5a.

Simulation research [47] and experimental work [48] of the temperature coefficient of the surface tension for the Fe–O binary metal showed that oxygen is a surface active element in the Fe–O system. The temperature coefficient of the surface tension ($d\sigma/dT$) is always negative for the Fe–O system with a low oxygen content. On the other hand, it changes from negative to positive when the oxygen content is over a critical value. Heiple et al. [6, 7] and Lu et al. [24, 25, 32–34] found that sulfur and oxygen are also active elements for stainless steel. When the active element content exceeds the critical value, the temperature coefficient of the surface tension ($d\sigma/dT$) changes from negative to positive, that is $d\sigma/dT > 0$, and the direction of the Marangoni convection on the weld pool changes in the manner as illustrated in Fig. 5b. In this case, the heat flux transfers from the center to the bottom and a relatively deep and narrow weld shape forms. The previous experimental results [24, 25] showed that when the oxygen content in the weld pool ranges from 70 to 300 ppm in SUS304 stainless steel, the temperature coefficient of the surface tension ($d\sigma/dT$) became positive.

The weld metal oxygen contents reach 68 and 82 ppm when the torch gas carbon dioxide content is at 0.4 and 0.5% for the 1 mm arc length as shown in Fig. 3. When the 3 mm arc length is employed, the weld metal oxygen content reaches 46 and 97 ppm with the torch gas carbon dioxide content of 0.1 and 0.2%, respectively, as shown in Fig. 4. Based on the results in Fig. 3 and 4, the critical value of the oxygen content in the weld pool to change the outward Marangoni convection to inward one should be between 68 and 82 ppm, which agrees well with the published data, 70 ppm. When the torch gas carbon dioxide content exceeds 0.4% for the 1 mm arc length and 0.2% for the 3 mm arc length as shown in Fig. 3 and 4, the weld metal oxygen content is over 70 ppm. In this case, the

Marangoni convection direction changes from outward to inward. Therefore, the weld shape changes from a relatively wide and shallow type (Fig. 1a–d and Fig. 2a, b) to a narrow and deep one (Fig. 1e–h and Fig. 2c–h), and the weld depth/width ratio (D/W) suddenly increases from 0.5 to 0.95 for the 1 mm arc length and 0.35 to 0.6 for the 3 mm arc length as shown in Figs. 3 and 4.

Figure 6 shows the weld depth comparison of the He–CO_2 shielding with Ar–CO_2 shielding under the inward Marangoni convection. It is obvious that the weld depth for the He–CO_2 mixed shielding is 2 mm deeper than that at the Ar–CO_2 mixed shielding with the same welding parameters of 160 A welding current, 2 mm s^{-1} welding speed, and 3 mm arc length. The stronger inward Marangoni convection on the pool surface and eletromagnetic convection in the liquid pool are considered to be the main factors that deepen the weld penetration with the He–CO_2 mixed shielding.

Effect of CO_2 on the arc voltage and weld shape

Table 2 shows the arc voltages for the 1 and 3 mm arc lengths with different CO_2 concentration in the He base shielding gas. Since the content of CO_2 is not over 1%, the variations in the arc voltages are small, between 14.2 and 15.0 V when the 1 mm arc length is used and between 18.3 and 19.2 V when the 3 mm arc length is employed. The ionization potential is 24.59 ev for He, which is higher than 13.77 ev for CO_2. Generally, addition CO_2 should decrease the arc voltage. However, in the experiments here, this effect is weak, especially for the 1 mm arc length, probably because of the low concentrations in the He base shielding gas. The large arc length will increase the arc voltage, which will increase the heat flux transferred to the weld pool and enlarge the weld width. Therefore, the weld pool volume and weld width for the 3 mm arc length are larger than that for the 1 mm arc length as shown in Figs. 1 and 2, which made the weld D/W ratio relatively small when the 3 mm arc length was used.

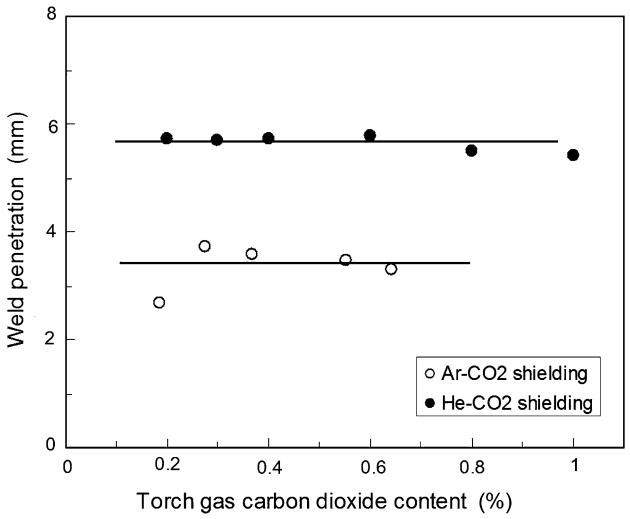

Fig. 6 Weld penetrations under He–CO_2 and Ar–CO_2 shielding

Table 2 Arc voltage at different He–CO_2 shielding and arc length (V)

Shielding gas	1 mm arc length	3 mm arc length
Pure He	14.5	19.2
He–0.1%CO_2	14.4	18.7
He–0.2%CO_2	14.6	18.3
He–0.3%CO_2	14.5	18.5
He–0.4%CO_2	14.6	18.6
He–0.6%CO_2	14.9	18.7
He–0.8%CO_2	14.8	18.9
He–1.0%CO_2	14.8	18.5

Carbon dioxide is an oxide gas. Adding an oxide gas in an inert shielding gas will increase the electrode consumption and cause the drop in the efficiency of TIG welding. The high oxygen content in the weld metal will cause the formation of oxide slag and void in the weld metal. Also the toughness of the weld metal for carbon steel decreases when the oxygen content is over 300 ppm [49]. Therefore, the addition of CO_2 to the inert gas should be controlled to less than 1%.

Effect of welding current on the weld shape

Figure 7 shows the effect of the welding current on the weld shape for He–0.6%CO_2 and pure He shielding at the constant welding speed of 2 mm s^{-1} and arc length of 1 mm. The weld is narrow and deep as shown in Fig. 7a–d when the He–0.6%O_2 shielding is used, and a relatively wide and shallow weld is obtained when pure He shielding is employed as shown in Fig. 7e–h. Figure 8 shows the weld depth/width (D/W) ratio and weld metal oxygen content for various welding currents. The weld metal oxygen content under pure He shielding is around 20 ppm and the outward Marangoni convection occurs, making the weld shape wide and shallow. When He–0.6%CO_2 shielding is used, the weld metal oxygen content is as high as 70–110 ppm and the inward Marangoni convection occurs on the liquid pool, thus forming deep and narrow welds as shown in Fig. 7a–d.

The weld D/W ratio slightly decreases with increasing welding current when pure He shielding is used. However, when He–0.6%CO_2 mixed shielding is employed, the weld D/W ratio initially increases with an increase in the welding current up to 180 A, and then decreases with the continuous increasing welding current. This fact is similar

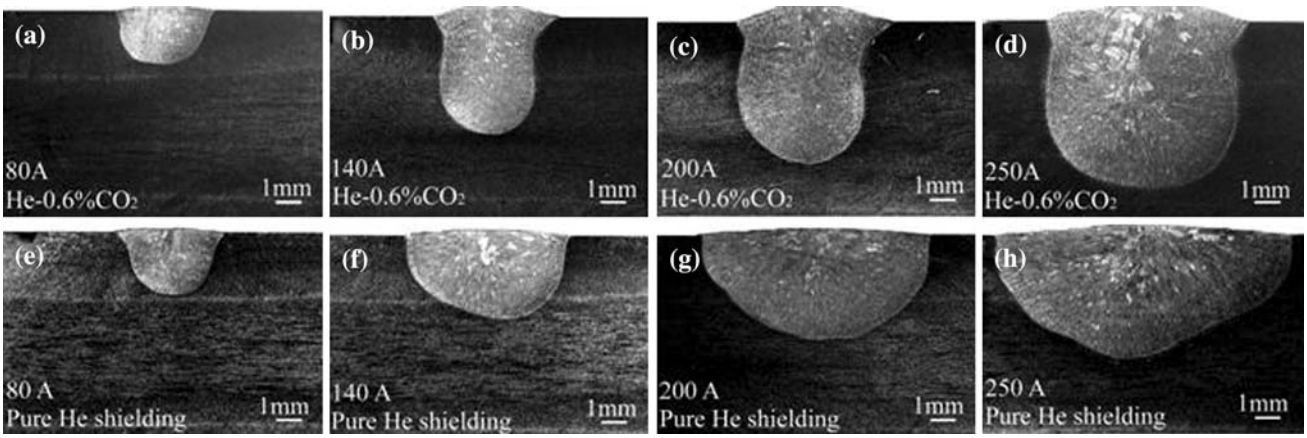

Fig. 7 Weld shapes at different welding current for pure He and He–0.6%CO_2 shielding gases

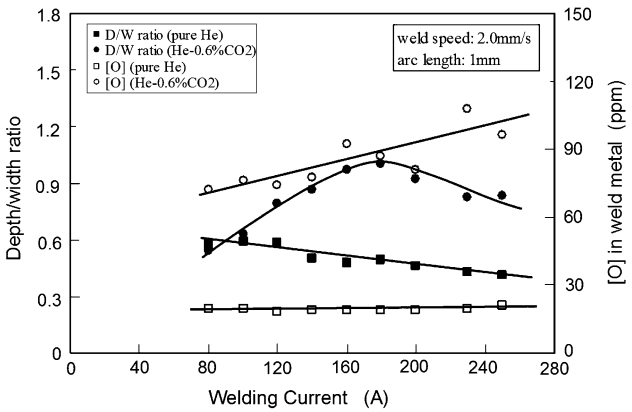

Fig. 8 Effect of welding current on weld shape and weld depth/width ratio under pure He and He–0.6%CO_2 shielding gases

to our published results for Ar–0.3%O_2 and Ar–0.3%CO_2 mixed shielding [33, 50], but different from the reported result under He–0.4%O_2 mixed shielding [35], where the weld D/W ratio continuously increases with the welding current.

Changing the welding current directly alters the heat input and the area of the weld. The heat distribution of the arc on the weld pool is the main factor affecting the weld shape and weld D/W ratio. Tsai and Eagar [51] observed that a high welding current raised the magnitude of the heat intensity and widens the heat distribution of the arc on the pool surface. However, the heat distribution width increases to a lesser extent than the magnitude of the heat density. The higher the magnitude of the heat density, the larger is the temperature gradient on the pool surface. Therefore, the Marangoni convection on the pool surface should be strengthened by the increasing welding current. Also, the high welding current should increase the magnitude of the electromagnetic convection in a liquid pool. The numerical study by Tanaka and Ushio [52, 53] of the GTA welding indicated that the convection flow in a liquid pool was mainly controlled by the Marangoni force and plasma drag force under pure Ar shielding. While under pure He shielding, the Marangoni force and electromagnetic force are the main factors controlling the convection in the liquid pool. When Ar–0.3%O_2 and Ar–0.3%CO_2 shielding are used, the plasma drag force which induces the outward convection in a liquid pool is one of the main factors affecting the weld shape. A higher welding current increases the plasma drag force and makes the weld D/W ratio slightly decrease or remain constant when Ar–0.3%O_2 or Ar–0.3%CO_2 shielding are used [33, 50]. When He–0.4%O_2 mixed shielding is employed, the high welding current directly strengthens the inward Marangoni convection on the pool surface and the inward electromagnetic convection in a liquid pool, which are the main forces controlling the pool convection for the He base shielded GTA welding. Therefore, the weld D/W ratio continuously increases with the increasing welding current for the He–0.4%O_2 shielding [35]. Here, it is interesting to find that the weld depth/width ratio initially increases with the welding current and then decreases when the welding current is over 180 A and He–0.6%CO_2 is used as shown in Fig. 8. It is assumed that the plasma drag force, which introduces the outward convection on the pool surface, plays a more important role than the Marangoni force and electromagnetic force under high welding currents, and hence the weld depth/width ratio decreases again at the high welding current with He–0.6%CO_2 shielding.

For pure He shielding, the outward Marangoni convection on a liquid pool occurs. The high welding current strengthens not only the outward Marangoni convection on the pool surface, but also the inward electromagnetic convection in a liquid pool. Through the interactive reaction of the two convections, the weld D/W ratio under pure He shielding is not sensitive to the welding current as shown in Fig. 8. A slight decrease in the weld D/W ratio with the increasing welding current also indicates that the

effect of the Marangoni convection is greater than that of the electromagnetic convection.

Effect of welding speed on the weld shape

Figure 9 shows the weld shapes for the different welding speeds from 0.75 to 5.0 mm s^{-1} at the constant welding current of 160 A and electrode tip work distance of 1 mm. All the weld shapes are narrow and deep when the He–0.6%CO_2 mixed shielding is used as shown in Fig. 9a–d, and wide and shallow weld shapes are formed for pure He shielding as shown in Fig. 9e–h. When the welding speed is 0.75 mm s^{-1} under the He–0.6%CO_2 shielding, a 9.7-mm weld penetration is obtained for single pass welding. Figure 10 shows the weld metal oxygen content and weld depth/width ratio (D/W) at different welding speeds for the pure He and He–0.6%CO_2 shieldings. For pure He shielding, the weld metal oxygen content is around 20 ppm, which is less than the value, 70–100 ppm. Therefore, the outward Marangoni convection for pure He shielding and the inward Marangoni convection for He–0.6%CO_2 occur on the liquid pool surface, respectively. The former one makes the weld shape wide and shallow as shown in Fig. 9e–h and the latter one makes it deep and narrow as shown in Fig. 9a–d. The weld D/W ratio at the He–0.6%CO_2 shielding decreases with increasing the welding speed, but it is not sensitive to the welding speed when pure He shielding is used.

The GTA weld shape for stainless steel depends to a large extent on the direction and magnitude of the Marangoni convection, which is determined by the product of the temperature coefficient of the surface tension (dσ/dT) and the temperature gradient (dT/dr) on the pool surface. Therefore, all the factors that affect the temperature

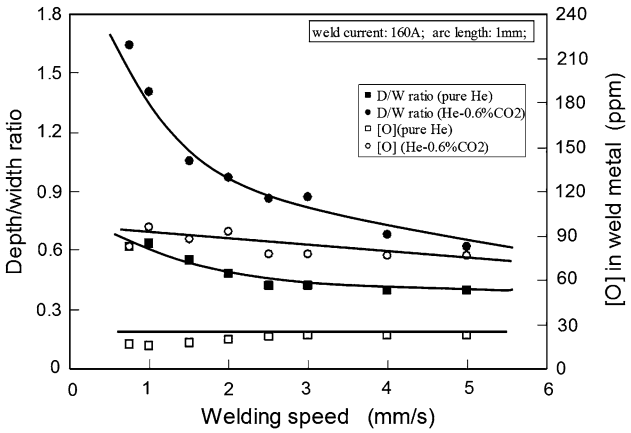

Fig. 10 Effect of welding speed on weld depth/width ratio and weld metal oxygen content under pure He and He–0.6%CO_2 shielding

coefficient of the surface tension (dσ/dT) or the temperature distribution on the pool surface govern the Marangoni convection in a liquid pool. The negative or positive sign of dσ/dT determines the Marangoni convection direction on the pool surface. The product of dσ/dT and dT/dr determines the magnitude of the Marangoni convection. In GTA welding, the peak temperature and temperature gradient on the pool surface are affected by the heat input distribution. A distributed heat source conduction model by Burgardt [54] showed that a slower welding speed increased the temperature gradient and the peak temperature on the pool surface. This was also experimentally recognized by Sundell [55]. Therefore, it is considered that increasing the welding speed decreases the peak temperature and the temperature gradient on the pool surface. A lower temperature gradient weakens the magnitude of the Marangoni convection on the pool surface. When the inward Marangoni convection occurs with He–0.6%CO_2 shielding, the

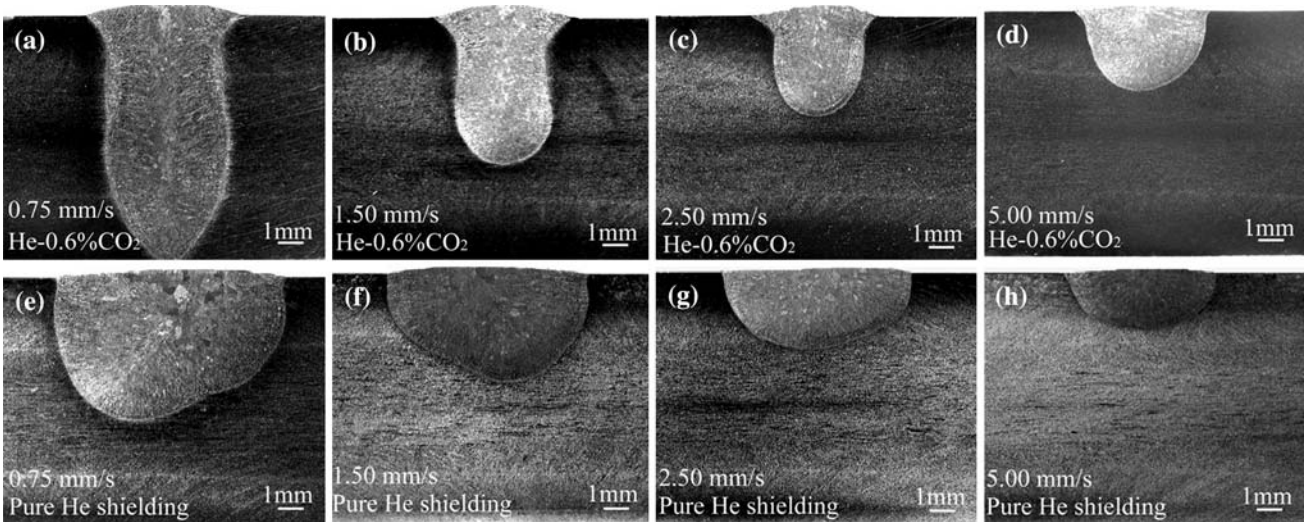

Fig. 9 Weld shapes at different welding speed for pure He and He–0.6%CO_2 shielding gases

inward Marangoni convection becomes weaker and the weld D/W ratio becomes smaller with increasing welding speed as shown in Fig. 10. However, for the outward Marangoni convection pattern for pure He shielding gas, the weak outward Marangoni convection reduces the weld width (W) and the radius of the weld pool surface (r). The smaller weld pool radius will increase the surface temperature gradient (dT/dr), and strengthen the magnitude of the outward Marangoni convection again. Therefore, the weld D/W is not sensitive to the welding speed for the outward Marangoni convection under pure He shielding as shown in Fig. 10. These results are in good agreement with the findings by Burgardt and Heiple [54], and Shirali and Mills [56] about the effect of the welding speed on the weld shape for stainless steel with different sulfur contents.

Conclusions

(1) The small addition of carbon dioxide to the He base shielding gas can significantly change the GTA weld shape from a wide shallow type to narrow deep one. Oxygen is an active element for SUS304 stainless steel, and can be precisely adjusted by the torch gas carbon dioxide content. When the torch gas carbon dioxide content exceeds 0.4% for the 1 mm arc length, the weld depth/width ratio suddenly increased from 0.5 to 0.95. When the 3 mm arc length is used, the weld depth/width ratio increased from 0.35 to 0.6 when the torch gas carbon dioxide content is over 0.2%.

(2) The GTA weld shape on stainless steel depends to a large extent on the pattern and magnitude of the Marangoni convection, which is controlled by the interactive effect of the weld metal oxygen content, the temperature coefficient of the surface tension ($d\sigma/dT$), and the temperature gradient on the pool surface. When the oxygen content in the weld pool exceeds a critical value from 68 to 82 ppm, the Marangoni convection changes from outward to inward suddenly on the pool surface. The welding parameters change the temperature gradient on the pool surface and resultantly change the magnitude of the Marangoni convection.

(3) For He–CO_2 mixed GTA welding, the liquid pool convection is mainly governed by the Marangoni force and the electromagnetic force. However, at high welding current, the arc plasma drag force also plays an important role and strengthens the outward convection on the pool surface, thus the weld depth/width ratio decreases at high welding currents with He–0.6%CO_2 shielding.

(4) For the slower welding speed of 0.75 mm s^{-1}, the welding current of 160 A and 1 mm arc length under the He–0.6%CO_2 shielding, the weld penetration reaches 9.7 mm for a single pass weld. The efficiency of the GTA welding can be significantly improved by the He–CO_2 mixed shielding compared to that under Ar–CO_2 mixed shielding.

Acknowledgements This study was supported by the New Energy and Industrial Technology Development Organization (NEDO) of Japan, the 21st Century COE Program, the ISIJ research promotion grant, JFE 21st Century Foundation and the Creative Fund of Institute of Metal Research, Chinese Academy of Science (IMR, CAS).

References

1. Lugwig H (1957) Weld J 36:335s
2. Savage WF, Nippes EF, Goodwin GM (1977) Weld J 56:126s
3. Oyler GW, Matuszesk RA, Carr CR (1967) Weld J 46:1006
4. Bennett WS, Mills GS (1974) Weld J 53:548s
5. Patton BE (1974) Autom Weld 27:1
6. Heiple CR, Ropper JR (1981) Weld J 60:143s
7. Heiple CR, Ropper JR (1982) Weld J 61:97s
8. Takeuchi Y,Takagi R, Shinoda T (1992) Weld J 71:283s
9. Gurevich SM, Zamkov VN (1966) Avtom Svarka 12:13
10. Kuo M,Sun Z, Pan D (2001) Sci Technol Weld Join 6:17. doi:10.1179/136217101101538497
11. Anderson PCJ, Wiktorowica R (1996) Weld Met Fabr 64:108
12. Lucas W, Howse D (1996) Weld Met Fabr 64:11
13. Schwemmer DD, Olson DL, Williamson DL (1979) Weld J 58:153s
14. Liu F, Lin S, Yang C, Wu L (2002) Trans Chin Weld Inst 23:1
15. Paskell T, Lundin C, Castner H (1997) Weld J 76:57
16. Liu F, Lin S, Yang C,Wu L (2002) Trans Chin Weld Inst 23:5
17. Wang Y, Tsai HL (2001) Metall Mater Trans B 32:501. doi:10.1007/s11663-001-0035-5
18. Tanaka M, Shimizu T, Terasaki H, Ushio M, Koshi-ishi F, Yang CL (2000) Sci Technol Weld Join 5:397. doi:10.1179/136217100101538461
19. Modenesi PJ, Apolimario ER, Pereira IM (2000) J Mater Process Technol 99:260. doi:10.1016/S0924-0136(99)00435-5
20. Fan D, Zhang RH, Gu YF, Ushio M (2001) Trans JWRI 30:35
21. Howse DS, Lucas W (2000) Sci Technol Weld Join 5:189. doi:10.1179/136217100101538191
22. Sire S, Marya S (2001) Proceedings of the 7th international symposium, Kobe, Japan, p 113
23. Sire S, Marya S (2001) Proceedings of the 7th international symposium, Kobe, Japan, p 107
24. Lu SP, Fujii H, Sugiyama H, Tanaka M, Nogi K (2002) Mater Trans 43:2926. doi:10.2320/matertrans.43.2926
25. Lu SP, Fujii H, Sugiyama H, Nogi K (2003) Metall Mater Trans A 34:1901. doi:10.1007/s11661-003-0155-4
26. Leconte S, Paillard P, Chapelle P (2007) Sci Technol Weld Join 12:120. doi:10.1179/174329307X159810
27. Rodrigues A, Loureiro A (2005) Sci Technol Weld Join 10:760. doi:10.1179/174329305X68769
28. Zhang RH, Fan D (2007) Sci Technol Weld Join 12:15. doi:10.1179/174329306X147535
29. Bad'yanov BN, Davdov VA, Ivanov VA (1974) Avtom Svarka 6:1
30. Bad'yanov BN (1975) Avtom Svarka 1:74
31. Heiple CR, Burgardt P (1985) Weld J 64:159s
32. Lu SP, Fujii H, Nogi K (2004) Mater Sci Eng A 380:290. doi:10.1016/j.msea.2004.05.057

33. Lu SP, Fujii H, Nogi K (2004) Scripta Mater 51:271. doi:10.1016/j.scriptamat.2004.03.004
34. Lu SP, Fujii H, Nogi K (2004) Metall Mater Trans 35A:2861
35. Lu SP, Fujii H, Nogi K, Sato T (2007) Quart J Jpn Weld Soc 25:196. doi:10.2207/qjjws.25.196
36. Savitskii MM, Leskov GI (1980) Avtom Svarka 9:17
37. Ludwig HC (1968) Weld J 47:234s
38. Ohji T, Make A, Tamura M, Inoue H, Nishiguchi K (1990) J Jpn Weld Soc 8:54
39. Kou S, Wang YH (1986) Weld J 65:63s
40. Heiple CR, Roper JR, Stagner RT, Aden RJ (1983) Weld J 62:72s
41. Fujii H, Sogabe N, Kamai M, Nogi K (2001) Proceedings of the 7th international symposium, Kobe, Japan, p 131
42. Leconte S, Paillard P, Chapelle P (2006) Sci Technol Weld Join 11:389. doi:10.1179/174329306X129544
43. Leconte S, Paillard P, Saindrenan J (2006) Sci Technol Weld Join 11:43. doi:10.1179/174329306X77047
44. Lowke JJ, Tanaka M, Ushio M (2004) The 57th annual assembly of international institute of welding, Osaka, Japan, IIW Doc 212-1053-04
45. Limmaneevichitr C, Kou S (2000) Weld J 79:231s
46. Kou S, Sun DK (1985) Metall Trans A 16:203
47. Sahoo P, Debroy T, Mcnallan MJ (1988) Metall Trans B 19:483. doi:10.1007/BF02657748
48. Taimatsu H, Nogi K, Ogino K (1992) J High Temp Soc 18:14
49. Ito Y, Nakanishi M, Konizo Y (1981) J Jpn Weld Soc 50:1211
50. Lu SP, Fujii H, Nogi K (2005) ISIJ Int 45:66. doi:10.2355/isijinternational.45.66
51. Tsai NS, Eagar TW (1985) Metall Trans B 16:841. doi:10.1007/BF02667521
52. Tanaka M, Terasaki H, Ushio M, Lowke JJ (2003) The 56th annual assembly of international institute of welding, Bucharest, Romania, IIW Doc 212-1040-03
53. Ushio M, Tanaka M, Lowke JJ (2004) IEEE Trans Plasma Sci 32:108. doi:10.1109/TPS.2004.823970
54. Burgardt P, Heiple CR (1986) Weld J 65:150s
55. Sundell RE, Solomon HD, Harris LP, Wojcik LA, Savage WF, Walsh DW (1983) Interim report to the national science foundation, General Electric Co., Schenectady, NY, SRD-83-006
56. Shirali AA, Mills KC (1993) Weld J 72:347s